Bull Math Biol
DOI 10.1007/s11538-017-0312-3

SPECIAL ISSUE : MATHEMATICAL ONCOLOGY

Simulating PDGF-Driven Glioma Growth and Invasion in an Anatomically Accurate Brain Domain

Susan Christine Massey[1] · **Russell C. Rockne** [2] · **Andrea Hawkins-Daarud**[1] · **Jill Gallaher**[3] · **Alexander R. A. Anderson**[3] · **Peter Canoll**[4] · **Kristin R. Swanson**[1]

Received: 2 August 2016 / Accepted: 16 June 2017

Abstract Gliomas are the most common of all primary brain tumors. They are characterized by their diffuse infiltration of the brain tissue and are uniformly fatal, with glioblastoma being the most aggressive form of the disease. In recent years, the over-expression of platelet-derived growth factor (PDGF) has been shown to produce tumors in experimental rodent models that closely resemble this human disease, specifically the proneural subtype of glioblastoma. We have previously modeled this system, focusing on the key attribute of these experimental tumors—the "recruitment" of oligodendroglial progenitor cells (OPCs) to participate in tumor formation by PDGF-expressing retrovirally transduced cells—in one dimension, with spherical symmetry. However, it has been observed that these recruitable progenitor cells are not uniformly distributed throughout the brain and that tumor cells migrate at different rates depending on the material properties in different regions of the brain. Here we model the differential diffusion of PDGF-expressing and recruited cell populations via a system of partial differential equations with spatially variable diffusion coefficients and solve the equations in two spatial dimensions on a mouse brain atlas using a flux-differencing numerical approach. Simulations of our in silico model demonstrate qualitative agreement with the observed tumor distribution in the experimental animal

✉ Susan Christine Massey
massey.susan@mayo.edu

1 Precision Neurotherapeutics Innovation Program, Mayo Clinic, 5777 E Mayo Blvd, Phoenix, AZ 85054, USA

2 Division of Mathematical Oncology, Department of Information Sciences, City of Hope, Duarte, CA, USA

3 Integrative Mathematical Oncology, Moffitt Cancer Research Center, Tampa, FL, USA

4 Division of Neuropathology, Department of Pathology and Cell Biology, Columbia University School of Medicine, New York, NY, USA

Published online: 25 August 2017

system. Additionally, we show that while there are higher concentrations of OPCs in white matter, the level of recruitment of these plays little role in the appearance of "white matter disease," where the tumor shows a preponderance for white matter. Instead, simulations show that this is largely driven by the ratio of the diffusion rate in white matter as compared to gray. However, this ratio has less effect on the speed of tumor growth than does the degree of OPC recruitment in the tumor. It was observed that tumor simulations with greater degrees of recruitment grow faster and develop more nodular tumors than if there is no recruitment at all, similar to our prior results from implementing our model in one dimension. Combined, these results show that recruitment remains an important consideration in understanding and slowing glioma growth.

Keywords Reaction–diffusion · Brain tumor · Glioma · Cancer · Platelet-derived growth factor (PDGF)

1 Introduction

Glioblastoma (GBM) is an aggressive cancer and is the most common primary brain tumor in adults. Malignant glioma cells are highly infiltrative of the normal surrounding tissue; however, the tumor cells rarely metastasize out of the central nervous system (CNS). The diffuse migration of tumor cells, combined with the complex spatial heterogeneity of brain tissue, leaves a large portion of the tumor cells invisible to clinical magnetic resonance imaging (MRI). This diffuse invasion is a hallmark of gliomas which presents many challenges for treatment and disease monitoring, particularly in the early stages of tumorigenesis, making in vivo and in silico tumor models especially important in gaining understanding of this disease.

Animal studies utilizing platelet-derived growth factor (PDGF) have provided improved models of glioma growth and evolution which recapitulate the diffuse, differential invasion of tumor cells within different regions of the brain (Assanah et al. 2006, 2009; Fomchenko and Holland 2007). These models demonstrate that a PDGF-expressing retroviral injection into neonatal or adult rodent brain will induce the formation of glioma-like tumors (Fig. 1) that appear histopathologically identical to human glioma (Assanah et al. 2006, 2009; Dai et al. 2001; Westermark et al. 1995). Moreover, use of retroviruses that express higher levels of PDGF drive the formation of more rapidly growing and higher-grade gliomas, which exhibit robust vascular proliferation and necrosis (Shih et al. 2004). Much of the rapid growth in this animal model is attributable to the observed phenomenon that oligodendroglial progenitor cells (OPCs) transduced with the PDGF-expressing retrovirus recruit other, untransduced OPCs (Assanah et al. 2006). OPCs express the platelet-derived growth factor receptor PDGFRα, enabling them to participate in autocrine and paracrine PDGF signaling loops with the PDGF secreted by the retrovirally transduced OPCs. Thus, the paracrine PDGF signal from the transduced OPCs to the untransduced OPCs causes the observed recruitment, whereby untransduced cells show increased proliferation and migration rates consistent with

cancer cells. These recruited OPCs contribute to the bulk of the tumor, comprising as much as 80–90% of the overall mass. The transduced OPCs respond likewise, reacting to the PDGF secreted by themselves and other nearby transduced OPCs, and make up the remaining 10–20% of the experimental tumor (Assanah et al. 2006).

To better understand the experimental results from these animal studies and their possible correlation to human disease, we previously adapted a reaction–diffusion model of glioma growth in humans (Harpold and Alvord 2007), which we refer to as the "Proliferation–Invasion" (PI) model, to include a recruitment process. This model, which we have termed the "Proliferation–Invasion–Recruitment" (PIR) model (Massey et al. 2012), consists of four coupled partial differential equations. In this previous work, we assumed a simplified homogeneous brain and solved our equations in one dimension with spherical symmetry. However, the experimental data (see Fig. 1) motivate a reaction–diffusion model for tumor growth and migration that includes tissue-dependent differential rates of diffusion. Moreover, it is understood that the migration rates of glioma cells along myelinated axons, which compose the white matter of the brain, are up to 100-fold faster than in the dense gray matter of neuronal bodies and dendrites that compose the cortex (Chicoine and Silbergeld 1995; Harpold and Alvord 2007). Thus, because glioma cells have been observed to move much more quickly along white matter tracts, migration not only depends on the local cellular density and the relative PDGF concentration gradient, which stimulates both migration and proliferation, but also upon the tissue properties.

To account for this and to ascertain the contribution of these differential diffusion rates, we have adapted our PIR model to run simulations on a two-dimensional mouse brain map. We then take the diffusion coefficient to be defined through a piecewise constant function, where both transduced and recruitable glial progenitor cells traveling in white matter take on a faster diffusion rate than those traveling in gray matter. We show that differential diffusion rates allow for better morphological agreement between simulation and experiment and that while these differential rates do

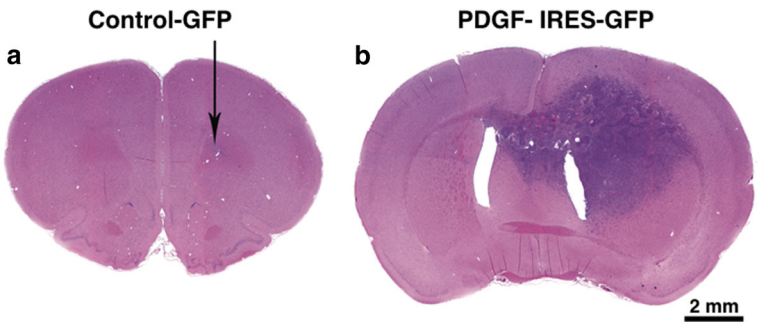

Fig. 1 Rodent brain slices. No tumors formed in rodents injected with control retrovirus, which lacked the PDGF-expressing region (**a**), yet tumors formed in 100% of rodents injected with PDGF-expressing retrovirus (**b**). The observed tumor shape in **b** suggests differential rates of tumor cell migration, with strong preference for migration along the myelinated axons across the corpus callosum. *Figure reproduced with permission from* Assanah et al. (2006)

not contribute largely to the overall speed of tumor growth, they do affect the relative preponderance of tumor cells (i.e., both transduced and recruitable OPCs) in the white and gray matter regions.

2 Proliferation–Invasion–Recruitment Model, in Two Spatial Dimensions

In the present model, there are three variables of interest: density of *transduced* cells (c) that over–express PDGF; density of untransduced *recruitable* oligodendroglial progenitor cells (r); and the concentration of PDGF (p). Our proliferation–invasion–recruitment (PIR) model equations account for the proliferation and diffusion of both transduced and recruitable OPCs, at rates $\rho_{c,r}$ and $D_{c,r}$, respectively, where the subscripts denote the relevant cell type. Additionally, it includes the production of PDGF by transduced cells and the consumption of PDGF by both cell types, at rates η_c and $q_{c,r}$, respectively. These contribute to the PDGF-driven recruitment of the recruitable OPCs by setting up localized gradients of PDGF, which can also diffuse at rate D_p. We schematizes the model in Fig. 2.

2.1 Model Equations

The equations for our model are as follows:

$$\overbrace{\frac{\partial c}{\partial t}}^{\substack{\text{rate of change}\\ \text{of transduced}\\ \text{cell density}}} = \overbrace{\nabla \cdot \left(\overline{D}_c\left(c, r, p, \mathbf{x}\right) \nabla c\right)}^{\substack{\text{net dispersal}\\ \text{of transduced cells}}} + \overbrace{\overline{\rho}_c\left(c, r, p\right) c}^{\substack{\text{net proliferation}\\ \text{of transduced cells}}} \tag{1}$$

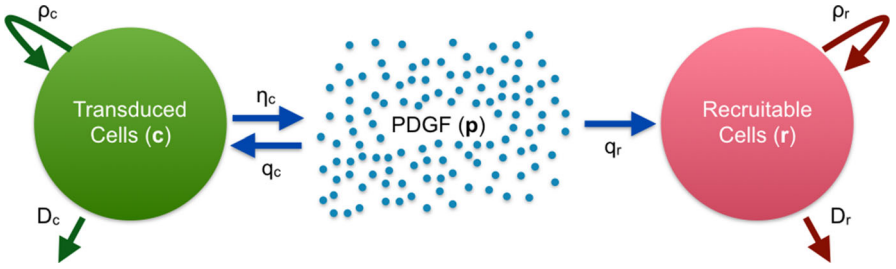

Fig. 2 Schematic representation of the model. Transduced cells (c, shown in *green*) produce PDGF (p, shown in *blue*) at rate η_c; PDGF (p) is consumed by both transduced (c) and recruitable (r, shown in *red*) glial progenitor cells at rates q_c and q_r, respectively. PDGF stimulates the proliferation and diffusion of infected glial progenitor cells at rates ρ_c and D_c, respectively, and that of uninfected progenitors at rates ρ_r and D_r. Note that PDGF molecules can also diffuse (at rate D_p, not illustrated). Equations relating these are given in Sect. 2.1, and Table 1 lists the parameters and the values used

$$\overbrace{\frac{\partial r}{\partial t}}^{\substack{\text{rate of change}\\ \text{of recruitable}\\ \text{cell density}}} = \overbrace{\nabla \cdot \left(\overline{D}_r\left(c, r, p, \mathbf{x}\right) \nabla r\right)}^{\substack{\text{net dispersal}\\ \text{of recruitable cells}}} + \overbrace{\overline{\rho}_r\left(c, r, p\right) r}^{\substack{\text{net proliferation}\\ \text{of recruitable cells}}} \tag{2}$$

$$\overbrace{\frac{\partial p}{\partial t}}^{\substack{\text{rate of change}\\ \text{of PDGF}\\ \text{concentration}}} = \overbrace{\nabla \cdot \left(D_p \nabla p\right)}^{\substack{\text{diffusion}\\ \text{of PDGF}}} + \overbrace{\eta_c c}^{\substack{\text{secretion}\\ \text{of PDGF by}\\ \text{transduced}\\ \text{cells}}} - \overbrace{q_r \beta\left(p\right) r}^{\substack{\text{consumption}\\ \text{of PDGF by}\\ \text{recruited}\\ \text{cells}}} - \overbrace{q_c \beta\left(p\right) \alpha c.}^{\substack{\text{consumption}\\ \text{of PDGF by}\\ \text{transduced}\\ \text{cells}}} \tag{3}$$

Equations (1)–(3) are reaction–diffusion equations describing the movement of cells and PDGF, as well as their synthesis, and in the case of PDGF, consumption. Notice that the diffusion and proliferation rates in (1) and (2) are density dependent and PDGF dependent. Accounting for these dependencies, the diffusion and proliferation rates take the form:

$$\overline{D}_c\left(c, r, p, \mathbf{x}\right) = D_c\left(\mathbf{x}\right) \frac{\beta\left(p + p_{\text{auto}}\right)}{\beta\left(\text{EC}_{50}\right) + \beta\left(p + p_{\text{auto}}\right)} \left(1 - \frac{c + r}{K}\right) \tag{4}$$

$$\overline{D}_r\left(c, r, p, \mathbf{x}\right) = D_r\left(\mathbf{x}\right) \frac{\beta\left(p\right)}{\beta\left(\text{EC}_{50}\right) + \beta\left(p\right)} \left(1 - \frac{c + r}{K}\right) \tag{5}$$

$$\overline{\rho}_c\left(c, r, p\right) = \rho_c \frac{\beta\left(p + p_{\text{auto}}\right)}{\beta\left(\text{EC}_{50}\right) + \beta\left(p + p_{\text{auto}}\right)} \left(1 - \frac{c + r}{K}\right) \tag{6}$$

$$\overline{\rho}_r\left(c, r, p\right) = \rho_r \frac{\beta\left(p\right)}{\beta\left(\text{EC}_{50}\right) + \beta\left(p\right)} \left(1 - \frac{c + r}{K}\right) \tag{7}$$

where the PDGF receptor binding kinetics are described by:

$$\beta\left(p\right) = \frac{p}{k_m + p} \tag{8}$$

$$\alpha = 1 - \beta(p_{\text{auto}}). \tag{9}$$

While these rates (4)–(7) look quite complicated, they can be broken down into three constituent parts: rate parameter, PDGF dependence, and density dependence. The density dependence ensures that we never exceed the carrying capacity. Although this is traditionally not needed in the diffusion term for a single species, in our model, the sum of both cell types is subjected to a single carrying capacity due to the spatial constraints of the brain, making this a necessary component in our cellular diffusion rate terms. Note that when space is limited, it is more difficult for cells to move past one another or to divide; thus, the slowing of migration and proliferation rates in such an environment is biologically realistic. PDGF dependence in our rates is motivated by experimental data, which demonstrate that the motility and cell division rates of OPCs are dependent on local PDGF concentration (Armstrong et al. 1990; Frost et al. 2009; Pringle et al. 1989). These rates are modulated both by PDGF receptor binding kinetics (that also modulate the PDGF consumption rates) and by what we call downstream dose-response. The PDGF receptor binding

kinetics given in (8) are based on Michaelis–Menten enzyme kinetics, with the traditional parameter k_m being the concentration of PDGF at which half of the maximal binding rate is achieved. However, this is insufficient to describe the downstream proliferation and migration dose responses to PDGF, leading to our derivation of the more complicated ratio of β's. This is explained more thoroughly in Massey et al. (2012), but essentially allows for the incorporation of the downstream dose response, with parameter EC_{50}, and the receptor binding, with parameter k_m, in a way that fits the data. The addition of the parameter p_{auto} allows us to include effects of autocrine signaling by transduced cells, which is also more thoroughly explained in Massey et al. (2012). Finally, the diffusion and proliferation rate parameters, $D_{c,r}$ and $\rho_{c,r}$, respectively, indicate the maximum attainable diffusion and proliferation rates. The proliferation rate parameters are fixed, but we allow the diffusion parameters to vary spatially, specifying different diffusion rates in gray versus white matter brain regions.

The rates of diffusion in (4) and (5) are functions of the spatial variable $\mathbf{x} = (x, y)$. It is assumed that these functions are piecewise constant depending on the local tissue properties, specifically, whether it is gray or white matter:

$$D_{c,r}(\mathbf{x}) = \begin{cases} D_{(c,r)} & \text{for } \mathbf{x} \in \text{white matter} \\ R_{wg} D_{(c,r)} & \text{for } \mathbf{x} \in \text{gray matter} \\ 0 & \text{for } \mathbf{x} \notin \text{brain tissue} \end{cases} \tag{10}$$

as is similarly done in proliferation–invasion (PI) model simulations implemented on a brain atlas (Swanson et al. 2000, 2002). Note, it is the atlas that delineates the gray and white regions of the brain. The unitless parameter R_{wg} represents the degree to which diffusion in white matter is faster than that in gray matter. We vary this parameter in simulations, with $R_{wg} > 1$, to see how this affects tumor growth in our model. $D_{c,r}$, R_{wg} and all other parameters are listed in Table 1.

The model equations we have presented here are more thoroughly derived in the supplemental material of Massey et al. (2012), where we developed a one-dimensional model of the experimental PDGF-driven tumors. However, the model presented here differs from that in Massey et al. (2012) in a few ways. First, by implementing our model in two dimensions we are able to incorporate different diffusion rates in gray versus white matter regions, as given by (10). Second, we have omitted chemotaxis. While there is evidence that OPCs chemotax in gradients of PDGF (Armstrong et al. 1990), there is also evidence that these cells move in response to PDGF in a way that is not chemotactic (Frost et al. 2009). Based on the cell tracking work we have done (Ivkovic et al. 2012; Massey et al. 2012), our analysis indicates that the movement of these cells can be mathematically modeled sufficiently using diffusion alone—therefore, taxis or directed migration terms, are not included. Finally, a third change is the lack of an equation for the remaining brain cells that do not actively participate in the formation of tumors. While these cells would contribute to the total cell density, we have made the simplifying assumption in both this model and our previous 1D model that they are passive and simply die as the tumor expands. This assumption made the contribution of these cells to the tumor dynamics negligible, as we

Table 1 Model parameters and their values

Symbol	Definition	Value	Units	Source
D_c	Max diffusion rate of transduced cells in gray matter	5.8×10^{-5}	$\frac{\text{cm}^2}{\text{day}}$	a
D_r	Max diffusion rate of recruited cells in gray matter	5.8×10^{-5}	$\frac{\text{cm}^2}{\text{day}}$	a
R_{wg}	Ratio of diffusion rates in white versus gray	10	Unitless	d
D_p	Diffusion rate of PDGF	5×10^{-4}	$\frac{\text{cm}^2}{\text{day}}$	a,b
ρ_c	Max proliferation rate of transduced cells	$\frac{\ln(2)}{18/24}$	day^{-1}	a
ρ_r	Max proliferation rate of recruited cells	$\frac{\ln(2)}{18/24}$	day^{-1}	a
η_c	Rate of PDGF secretion by transduced cells	10^{-5}	$\frac{\text{ng/cell}}{\text{day}}$	a
q_c	Max rate of PDGF uptake by transduced cells	$10^{-5.15}$	$\frac{\text{ng/cell}}{\text{day}}$	a
q_r	Max rate of PDGF uptake by recruited cells	$10^{-5.15}$	$\frac{\text{ng/cell}}{\text{day}}$	a
K	Cellular carrying capacity	2.3×10^8	$\frac{\text{cells}}{\text{mL}}$	a
k_m	[PDGF] at which half max binding occurs	30	$\frac{\text{ng}}{\text{mL}}$	a,c
EC_{50}	[PDGF] achieving half max dose response	$10^{1/2}$	$\frac{\text{ng}}{\text{mL}}$	a,c
p_{auto}	Autocrine PDGF level for transduced cells	1	$\frac{\text{ng}}{\text{mL}}$	a
$O2a$	Baseline population of OPCs in gray matter	2.2×10^6	$\frac{\text{ng}}{\text{mL}}$	a

The derivation of most parameters can be found in Massey et al. (2012) and its supplemental material. Many are experimentally derived, or came from a combination of literature sources and testing in simulations

[a] Massey et al. (2012)

[b] Thorne et al. (2004)

[c] Pringle et al. (1989)

[d] Note that the value given here for R_{wg} comes from varying the parameter in simulations, as described in the results (Sect. 3)

found that removing this population from our 1D model did not alter the simulation results. Additionally, our assumption is biologically realistic, since the carrying capacity of the brain is approximately three times the normally observed average cellular density of the brain. Invading tumor cells would deplete resources and cause these non-tumor cells to die off before the total cell population nears the carrying capacity.

2.2 Initial and Boundary Conditions

Initial Conditions To set the initial conditions for this problem, we take the baseline population of glial progenitor cells (OPCs) in normal healthy brain tissue (given by parameter $O2a$), and define a spherical region around the site of the injection wherein we assume that most (99%) of these progenitor cells are infected:

$$c(\mathbf{x} = \mathcal{R}, t = 0) = \begin{cases} 0.99 \cdot O2a(\mathbf{x}) & \text{for } \mathcal{R} < 0.03 \text{ cm} \\ 0 & \text{else} \end{cases} \tag{11}$$

where

$$\mathcal{R}^2 = (x - x_{\text{injection}})^2 + (y - y_{\text{injection}})^2 \tag{12}$$

is the radial distance from the injection site $(x_{\text{injection}}, y_{\text{injection}})$.

Any OPCs inside or outside of this region that are not infected following the injection, and thus not transduced, are considered to be "recruited" and "recruitable" cells, respectively.

$$r(\mathbf{x} = \mathcal{R}, t = 0) = \begin{cases} 0.01 \cdot O2a(\mathbf{x}) & \text{for } \mathcal{R} < 0.03 \text{ cm} \\ O2a(\mathbf{x}) & \text{else.} \end{cases} \tag{13}$$

Note that $O2a(\mathbf{x})$ is spatially dependent, since there are more OPCs in white matter than in gray matter. In practice, we let $O2a$ represent the density of these cells in gray matter and set $8/3 \cdot O2a$ to represent the density in white matter, since OPCs make up approximately 3% of the normal gray matter and about 8% of the normal white matter (Nunes et al. 2003; Rhee et al. 2009; Roy et al. 1999):

$$O2a(\mathbf{x}) = \begin{cases} O2a & \mathbf{x} \in \text{gray matter} \\ \frac{8}{3} O2a & \mathbf{x} \in \text{white matter.} \end{cases} \tag{14}$$

The injection site for our simulations was chosen by determining the approximate center of the tumor in Fig. 1b and selecting a similar location in the computational domain specified by the brain atlas.

For the initial PDGF concentration, we take

$$p(\mathcal{R}, 0) \equiv 0$$

since we assume that there is no PDGF in the tissue until it is secreted by the transduced cells. In reality, there may be some small amount released in response to the injury induced by injecting the brain; however, we assume that to be negligible.

Boundary Conditions The physical boundary conditions of the problem are no-flux of tumor cells outside of the brain $\mathcal{B}$, so that

$$\nabla q \cdot \mathbf{n} = 0 \tag{15}$$

where $q = [c, r, p]'$ and $\mathbf{n}$ is the vector normal to the boundary $\partial\mathcal{B}$.

Computational Domain We utilize a brain atlas (Ma et al. 2005, 2008) to define our computational domain. This atlas specifies, on a Cartesian grid with resolution 0.01 cm, the gray and white regions inside the brain where the tumor may grow, as well as the ventricles and anything outside the brain where it does not. (The brain atlas we used is open source; details may be found online at http://brainatlas.mbi.ufl.edu.)

2.3 Numerical Method

To implement our model, we use a fractional step approach. First, we use Godunov operator splitting to solve the reaction and diffusion terms in two separate steps. Further, we split the spatial dimensions to turn our two-dimensional problem into a sequence of two locally one-dimensional (LOD) problems. At each iteration of our method, we first solve the diffusion component, coupling the LOD technique with the Crank Nicholson (CN) method. This allows us to solve in the x- and then the y-directions in two sweeps, rather than using a ten point CN stencil, greatly increasing computational efficiency. Next, we solve the reaction terms using the TRBDF2 method (that is, the two-stage Runge–Kutta method combining the trapezoidal rule with the second-order backward differentiation formula). Further detail about how this was implemented in code form can be found at: https://github.com/scmassey/2D_Proliferation-Invasion-Recruitment. Additional details about these numerical methods can be found in LeVeque (2002, 2007). We remark that despite the discontinuous diffusion coefficient, no jump conditions were formally introduced. This decision is supported by an analysis of the differential diffusion rates in the PI model across the gray–white interface that was done in Belmonte-Beitia et al. (2013) where the authors showed solutions of this model would be smooth and would not have a build up of cells on either side of such a discontinuity.

2.4 Comparing Simulated Tumor Growth

Because gliomas are diffuse, lacking a defined edge, we compare simulated tumors of similar size by looking at a region defined by a density threshold. For the PI model (Harpold and Alvord 2007), we commonly focus on the region where the cell density is $\geq$80% of the carrying capacity, since this corresponds with the hypercellular region of tumor that is visible on T1-weighted MRI with Gadolinium contrast agent (T1Gd MRI). Therefore, we chose to use this density for comparing our PIR model simulated tumors. Additionally, rather than describing the size of these regions as an area, we instead use the circular equivalent radius. Solutions of this model are known to asymptotically approach a linear radial growth profile in homogeneous conditions. Therefore, it is natural to compare simulated tumors at various time points with their circular equivalent radii. Throughout the results, we will denote a circular equivalent radius that corresponds to the region where the cellular density is $\geq$ 80% of carrying capacity as the "80% radius" or "80% circular equivalent radius."

For comparing growth in specific regions of the tumor, we set up two particular axes originating at the center of the tumor (where the simulated tumor was initiated). One such axis is vertical, passing through the white matter portion of the brain atlas, and the other is horizontal, remaining strictly in the gray matter portion of the atlas. Having these axes passing through the different regions enables us to see how cell densities are affected by the differential diffusion rate in these two tissues.

3 Simulation Results

3.1 Qualitative Match Between 2d Simulation and Experimental Tumor

Simulations of the two-dimensional PIR model display qualitatively similar patterns of tumor invasion as those observed in the experimental murine system (Fig. 3). In particular, the gray and white matter heterogeneity allows for good overall morphological agreement with experimental murine tumors. The former one-dimensional model only simulated tumors to grow in a spherical shape, while the experimental tumors show a clear preference for growing along white matter tracts (Fig. 3a). The addition of both the spatially heterogeneous initial condition for recruitable OPCs (Sect. 2.2) and the differential cellular diffusion rate in gray versus white matter (Eqs. 10) contributes to the improved agreement between model simulations and the spatial distribution of tumor cells in the animal model. Note that because we can only approximate the histological slice with a slice from the atlas, we cannot register the simulation to histology images. Thus, a quantitative comparison would not be more informative than a visual qualitative comparison.

Varying the ratio of the diffusion rates in white and gray matter, R_{wg}, we determined that the 10-fold higher diffusion rate that has been used in PI model simulations of human tumors results in the best agreement between simulation and histology. Values of R_{wg} smaller than 10 look more circular, and values of R_{wg} greater than 10 appear to travel much further along the white matter tracts (see Figs. 6 or 7 for examples

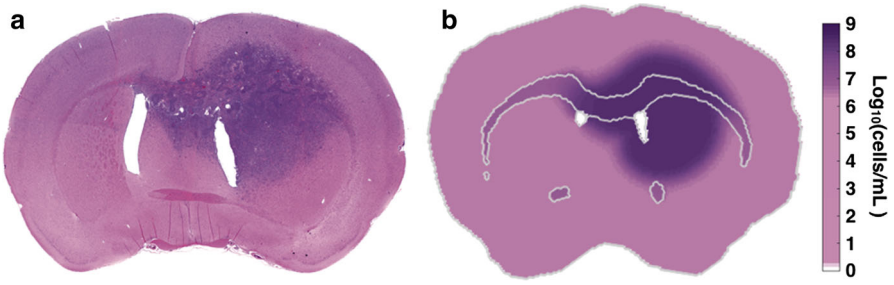

Fig. 3 Comparison of simulated tumor and hematoxylin and eosin (H&E) of experimental PDGF-driven tumor. **a** Tissue slice from an experimental PDGF-driven tumor stained with H&E, *reproduced with permission from* Assanah et al. (2006). **b** Simulated tumor using our 2D PIR model implemented on a rodent brain atlas, with parameter $R_{wg} = 10$. *Color bar* is on a log scale and shows the total density of recruitable and transduced cells. *Gray* outlined region in the middle shows the corpus callosum. The *purple* region shows the area where the tumor resides, while the *pink* is primarily reflective of the baseline density of recruitable cells

of simulations with lower and higher values of R_{wg}). The effects of varying R_{wg} are explored more in Sect. 3.3.

3.2 PDGF Secretion Rates Positively Correlate with Tumor Growth Rates and Nodularity

We simulated tumors with different values of PDGF secretion rate, η_c, for 30 days and then compared results at that time point to look at how this parameter affects the speed of overall tumor growth. Our results show that the tumors with little or no PDGF secretion are significantly smaller than those with moderate or high PDGF secretion (Fig. 4a–c). This demonstrates that PDGF secretion, and thus recruitment, greatly contributes to the speed at which these tumors grow, with higher secretion resulting in fast-growing tumors, and low secretion resulting in relatively slow-growing tumors.

Next, we compared tumor simulations with the different rates of PDGF secretion (i.e., different values of η_c) at the same size, as determined by their 80% circular equivalent radii. To do this, we simulated tumors until they had a circular equivalent radius of 0.2 cm (2 mm) at the 80% density threshold as described in Sect. 2.4. This comparison reveals that the tumors with less recruitment are more diffuse (Fig. 5). Specifically, the tumor with no PDGF secretion, and thus no recruitment, has a more extensive region of tumor extending beyond the $\geq$80% density threshold, showing the greatest degree of diffuse invasion. The tumor with the most recruitment (on the right) has the least amount of tumor extending beyond this 80% density threshold, making it the least diffusely invasive.

In the aforementioned simulations and associated figures, we did not vary R_{wg} but held it fixed at 10 (as discussed in Sect. 3.1). This enabled us to examine the spatially dependent changes that occur due to tumor growth in gray versus white matter brain regions without the additional signal of varied magnitude. Looking across two different axes of the tumor, one in gray matter only, and the other passing through the white matter (labeled x and y, respectively, in both Figs. 4 and 5), we can see the effect of having a differential diffusion rate upon the cellular density and the proportion of tumor that is made up of recruited cells. In the white matter, we see that the tumor cell density curve is less steep due to increased diffusion in this region (compare Fig. 4c with b, and likewise, Fig. 5c with b). There is also a slight increase in cell density in this region due to the presence of more background recruitable cells in the white matter. Correspondingly, the proportion of tumor made up by recruited cells is a bit higher at the leading "edge" when it is in white matter (compare Fig. 5e with d), while increases are less steep in this region (compare Fig. 4e with d). This is likely due to both the increase in background recruitable cells in the white matter, as well as the increased invasion rate of transduced cells happening at the "edge"—the transitional zone from dense tumor to normal brain, where there are mostly only recruitable OPCs (recruited fraction near 1)—when it passes through the white matter region. Note that the increases in Fig. 5d, e for the curves at approximately 0.3 cm is due to cells diffusing out of the corpus callosum, just beyond the left end of the axis labeled x, into the gray matter. That is, cells and PDGF diffusing toward the right out of the corpus callosum increase the number of recruited cells in that region.

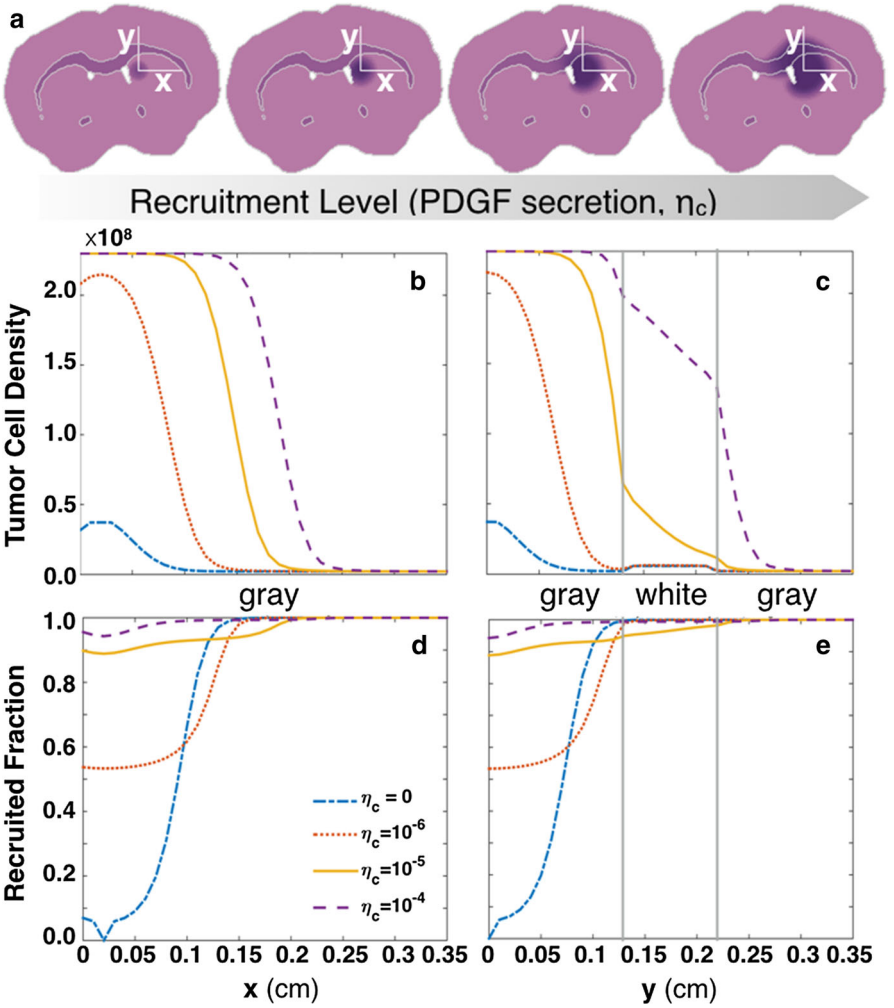

Fig. 4 Tumors of varying degrees of recruitment simulated for same length of time (30 days). **a** Simulated tumors at 30 days of growth, with different values for parameter η_c to simulate varied recruitment (from *left to right*: $\eta_c = 0, 10^{-6}, 10^{-5}$, and 10^{-4} ng/cell/day, respectively). *White lines* labeled x and y show the locations from which we sampled the cellular densities that are plotted in panels **b**–**e**; these correspond to the x and y labels underneath those panels. These start at the center where the simulation was initialized, then x extends out in only gray matter, while y extends through the corpus callosum (white matter), as indicated by the *vertical lines* in **c** and **e**. **b** Cell densities versus space, sampled in an exclusively gray matter region. **c** Cell densities versus space, sampled in a region that passes through white matter (*vertical lines*). **d** Fraction of tumor that is made up of recruited progenitor cells versus space. **e** Fraction of tumor that is made up of recruited cells versus space, passing through white matter (*vertical lines*)

3.3 Influence of Differential Gray Versus White Matter Diffusion Rates

To better understand the contribution of differential rates of diffusion in gray versus white matter, R_{wg}, as separate from that of PDGF secretion rate, η_c, we ran a series of simulations varying both independently. We ran 16 simulations, with four values

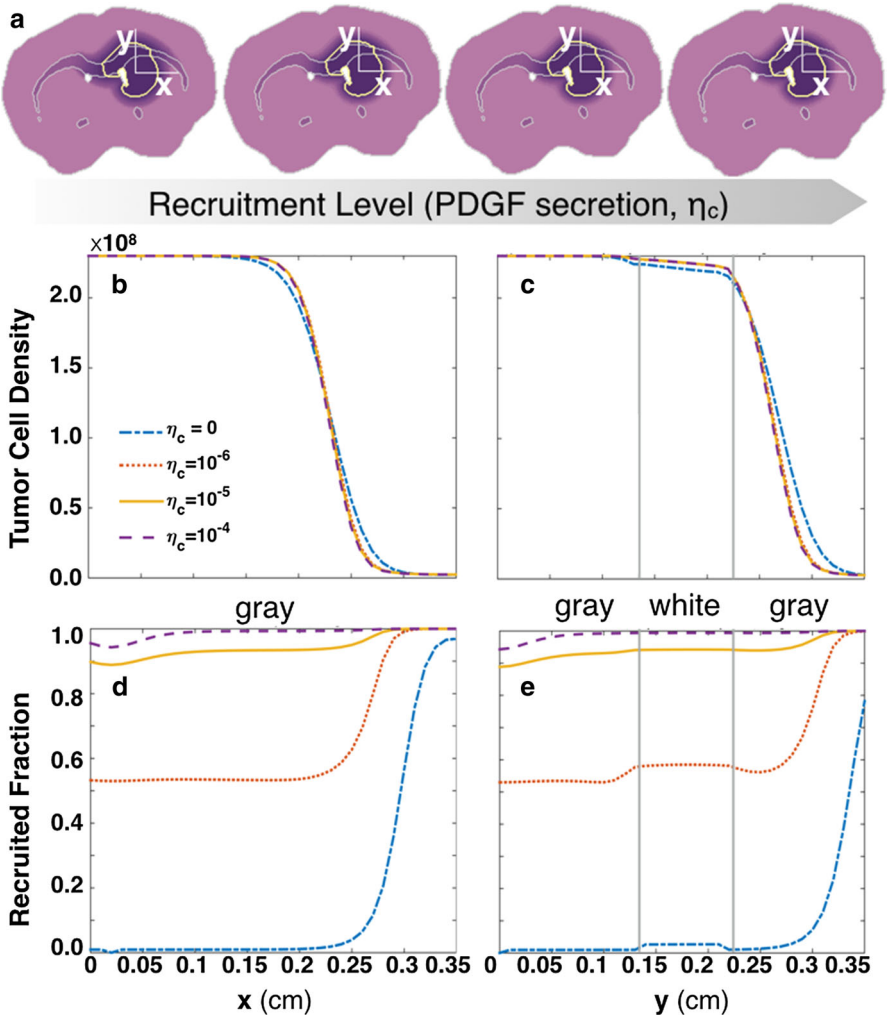

Fig. 5 Tumors of varying degrees of recruitment simulated until reaching same 80% circularly equivalent radius (0.2 cm). Simulated tumors with a circular equivalent radius of 0.2 cm at the ≥80% density threshold (see Sect. 2.4), having different values of η_c to indicate varying degrees of recruitment (from *left to right*: $\eta_c = 0, 10^{-6}, 10^{-5}$, and 10^{-4} ng/cell/day, respectively). The region of cell density ≥80% of carrying capacity is outlined in *yellow*. *White lines* labeled *x* and *y* show the locations from which we sampled the cellular densities that are plotted in panels **b**–**e**; these correspond to the *x* and *y* labels underneath those panels. These start at the center where the simulation was initialized and then *x* extends out in only gray matter, while *y* extends through the corpus callosum (white matter), as indicated by the *vertical lines* in **c** and **e**. **b** Cell densities versus space, sampled in gray matter region. **c** Cell densities versus space, sampled through white matter (*vertical lines*). **d** Fraction of tumor that is made up of recruited progenitor cells versus space, staying in only gray matter. **e** Fraction of tumor that is made up of recruited progenitor cells versus space, passing through white matter (*vertical lines*)

of R_{wg} and four values of η_c, and compared the results at similar tumor sizes (at the 80% density threshold described in Sect. 2.4). We then focused comparisons on two outcomes where we expected both parameters to play a significant role. In the first,

we looked at the fraction of total tumor residing in the white matter regions of the brain. The second comparison examined the time required for the tumors to reach the specified size, essentially indicating the speed of growth.

Our first comparison shows that the fraction of tumor cells in white matter regions increases both with increasing R_{wg} and with increasing η_c, as expected. However, at most sizes we observe that it is much more strongly affected by R_{wg} (Fig. 6). At large tumor sizes, the fraction decreases, corresponding to the tumor growing beyond the size of the white matter regions. Note that because our simulations step in time, we chose for each heatmap the first time point at which a simulated tumor was greater than or equal to the specified size. Thus, not all simulated tumors are precisely the same size in the heatmaps. In the case of the heatmap of tumors with 0.1 cm 80% radius, where the "edge" of the tumor is very close to the corpus callosum, the variations in size could result in a significant increase in the number of cells in the white matter. This is likely the cause for the disruption, in this particular heatmap, of the pattern observed in Fig. 6. Overall, the relationship between the fraction of tumor in white matter and R_{wg} suggests that tumors showing a proclivity for white matter regions may have greater differential rates of cellular diffusion in white matter than in gray.

In our second comparison, we examined time duration of growth required to reach specific sizes at the 80% of carrying capacity density threshold described in Sect. 2.4. We see that both R_{wg} and η_c correspond with faster growth, but that η_c is the more influential parameter (Fig. 7). These heatmaps show that the speed of these tumors' growth depends highly on the rate of PDGF secretion and thus the degree of recruitment. This relationship is particularly pronounced at smaller tumor sizes, where R_{wg} appears to have very little effect. At extremely large tumor sizes, where the size of the dense tumor core approaches the size of the brain itself, R_{wg} appears to play a greater role in contributing to this speed of growth. However, this is likely of little practical importance, since tumors are typically lethal prior to reaching such large sizes. The result that recruitment plays a significant role in the growth rate of tumors suggests that reducing PDGF signal, perhaps through use of PDGF inhibitor therapies or other drugs targeting the PDGF pathway, could greatly slow the growth of tumors that show a high degree of OPC recruitment.

4 Discussion

We have shown that our reaction–diffusion PDE model for glioma growth reproduces the growth patterns observed in vivo (Fig. 3). The morphology of the tumor growth depends critically on differential rates of migration of tumor cells through the brain. Without the differential rates, we would obtain spherical symmetry equivalent to that in the one-dimensional PIR model (Massey et al. 2012). Moreover, the degree to which the rate of diffusion in white matter exceeds that of gray matter can greatly affect the shape and location of the tumor cells (Figs. 6, 7). Our simulations show that having greatly different diffusion rates in these regions can lead to tumors that fill the entire corpus callosum of the brain within a short period of time. Interestingly, this is consistent with observations from human patients, some of whom have

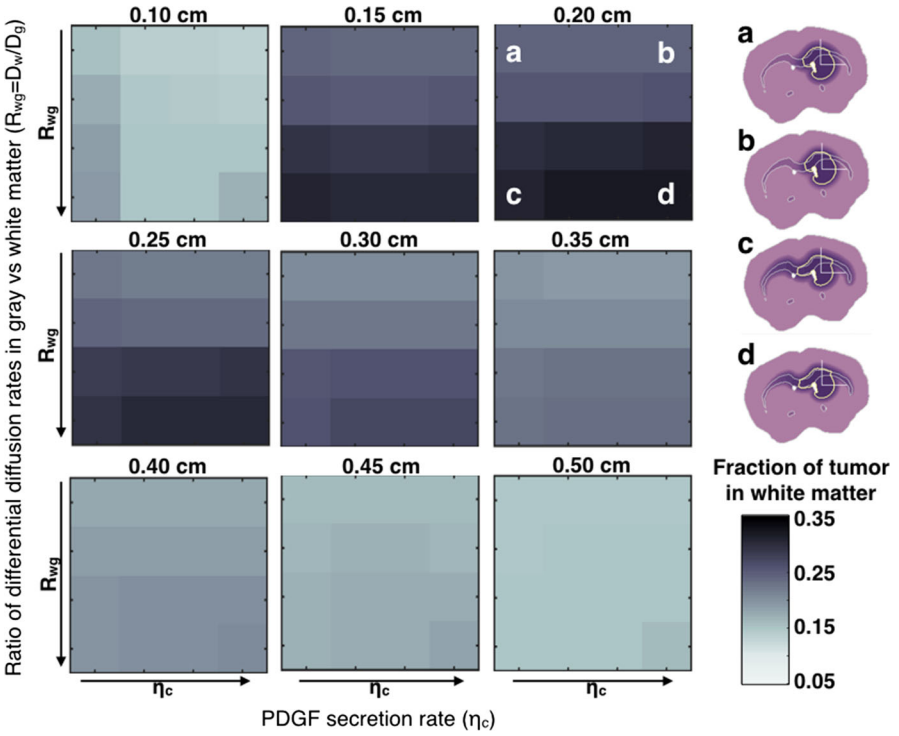

Fig. 6 Fraction of tumor cells in white matter regions at indicated sizes for varied ratios, R_{wg}, of differential cellular diffusion rates and varied PDGF secretion rates, η_c. Each heatmap relates to a different 80% radius (see Sect. 2.4), as indicated above the heatmap. *Arrows* show direction of increasing parameter values: going down the columns of each heatmap, we have $R_{wg} = 5$, 10, 50, and 100, and from *left to right* along the rows we have $\eta_c = 0$, 10^{-6}, 10^{-5}, and 10^{-4} ng/mL/day. The *color map* indicates the fraction of tumor that is in white matter structures as opposed to gray matter. The four tumor simulations shown **a**–**d** correspond with the combinations of the high and low extreme values of these two parameters, R_{wg} and η_c, at the point when they each have a 0.2-cm 80% circular equivalent radius

tumors that are said to display a "preference" for white matter, or whose tumors are described as "white matter disease." Prior to our results, we supposed that recruitment might play an important role in this, since there are more recruitable OPCs in white matter regions. Based on the results we found, however, we would hypothesize that the observation of "white matter disease" in human patients could also be related to a high ratio of tumor cell motility rates in white matter as compared to gray.

Additionally, we found that OPC recruitment results in a less-diffuse, faster-growing tumor, which is consistent with what we found using the one-dimensional spherically symmetric PIR model (Massey et al. 2012). Importantly, we observe that this impact on growth rate is preserved over a broad range of differential diffusion rates between gray and white matter (Figs. 4, 5). This suggests that recruitment is a significant factor to consider in slowing the growth of these experimental tumors, and possibly in the proneural human glioblastomas they resemble. That is, these results suggest that more rapidly growing untreated human tumors might be more likely to show recruitment

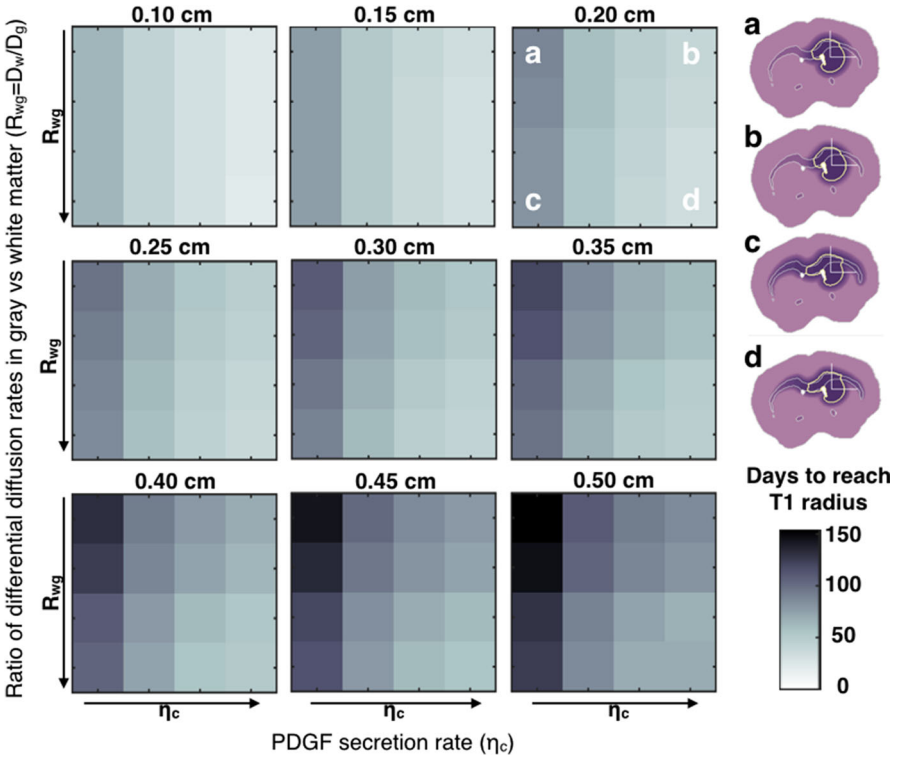

Fig. 7 Growth time required to reach indicated sizes for varied ratios, R_{wg}, of differential cellular diffusion rates and varied PDGF secretion rates, η_c. Each heatmap relates to a different 80% radius (see Sect. 2.4), as indicated above the heatmap. *Arrows* show direction of increasing parameter values. Going down the columns of each heatmap, $R_{wg} = 5$, 10, 50, and 100, and from *left to right* along the rows $\eta_c = 0$, 10^{-6}, 10^{-5}, and 10^{-4} ng/mL/day. The *color map* indicates the time (in days) required to reach the indicated size. The four tumor simulations shown **a**–**d** correspond with the combinations of the high and low extreme values of R_{wg} and η_c, at the point when they each have a 0.2-cm 80% circular equivalent radius

of oligodendroglial progenitor cells. Interrupting the paracrine signaling that leads to recruitment could then be key to slowing the growth of these more rapidly growing tumors, leading to longer patient survival times.

Acknowledgements This material is based upon work supported by the National Science Foundation Graduate Research Fellowship Program under Grant No. DGE-0781824, by the National Institutes of Health under awards R01NS060752, U54CA143970, and R01CA164371, and by the James S. McDonnell Foundation Collaborative Activity Award #220020264. The content is solely the responsibility of the authors. Any opinions, findings, and conclusions or recommendations expressed in this material are those of the authors and do not necessarily reflect the views of the National Science Foundation, the National Institutes of Health, or the James S. McDonnell Foundation.

References

Armstrong RC, Harvath L, Dubois-Dalcq ME (1990) Type 1 astrocytes and oligodendrocyte-type 2 astrocyte glial progenitors migrate toward distinct molecules. J Neurosci Res 27(3):400–407. doi:10.1002/jnr.490270319

Assanah M, Lochhead R, Ogden A, Bruce J, Goldman J, Canoll P (2006) Glial progenitors in adult white matter are driven to form malignant gliomas by platelet-derived growth factor-expressing retroviruses. J Neurosci 26(25):6781–6790. doi:10.1523/jneurosci.0514-06.2006

Assanah MC, Bruce JN, Suzuki SO, Chen A, Goldman JE, Canoll P (2009) PDGF stimulates the massive expansion of glial progenitors in the neonatal forebrain. Glia 57(16):1835–1847. doi:10.1002/glia.20895

Belmonte-Beitia J, Woolley TE, Scott JG, Maini PK, Gaffney EA (2013) Modelling biological invasions: individual to population scales at interfaces. J Theor Biol 334:1–12 doi:10.1016/j.jtbi.2013.05.033

Chicoine MR, Silbergeld DL (1995) Assessment of brain tumor cell motility in vivo and in vitro. J Neurosurg 82(4):615–622. doi:10.3171/jns.1995.82.4.0615

Dai C, Celestino JC, Okada Y, Louis DN, Fuller GN, Holland EC (2001) PDGF autocrine stimulation dedifferentiates cultured astrocytes and induces oligodendrogliomas and oligoastrocytomas from neural progenitors and astrocytes in vivo. Genes Dev 15(15):1913–1925. doi:10.1101/gad.903001

Fomchenko EI, Holland EC (2007) Platelet-derived growth factor-mediated gliomagenesis and brain tumor recruitment. Neurosurg Clin N Am 18(1):39–58. doi:10.1016/j.nec.2006.10.006

Frost EE, Zhou Z, Krasnesky K, Armstrong RC (2009) Initiation of oligodendrocyte progenitor cell migration by a PDGF-A activated extracellular regulated kinase (ERK) signaling pathway. Neurochem Res 34(1):169–181. doi:10.1007/s11064-008-9748-z

Harpold HL, Alvord EC Jr, Swanson KR (2007) The evolution of mathematical modeling of glioma proliferation and invasion. J Neuropathol Exp Neurol 66(1):1–9. doi:10.1097/nen.0b013e31802d9000

Ivkovic S, Beadle C, Noticewala S, Massey SC, Swanson KR, Toro LN, Bresnick AR, Canoll P, Rosenfeld SS (2012) Direct inhibition of myosin II effectively blocks glioma invasion in the presence of multiple motogens. Mol Biol Cell 23(4):533–542. doi:10.1091/mbc.e11-01-0039

LeVeque RJ (2002) Finite volume methods for hyperbolic problems. Cambridge University Press, Cambridge

LeVeque RJ (2007) Finite difference methods for ordinary and partial differential equations: steady-state and time-dependent problems. SIAM, Philadelphia

Ma Y, Hof PR, Grant SC, Blackband SJ, Bennett R, Slatest L, McGuigan MD, Benveniste H (2005) A three-dimensional digital atlas database of the adult c57bl/6j mouse brain by magnetic resonance microscopy. Neuroscience 135(4):1203–1215. doi:10.1016/j.neuroscience.2005.07.014

Ma Y, Smith D, Hof PR, Foerster B, Hamilton S, Blackband SJ, Yu M, Benveniste H (2008) In vivo 3d digital atlas database of the adult c57bl/6j mouse brain by magnetic resonance microscopy. Front Neuroanat.10.3389/neuro.05.001.2008

Massey SC, Assanah MC, Lopez KA, Canoll P, Swanson KR (2012) Glial progenitor cell recruitment drives aggressive glioma growth: mathematical and experimental modelling. J R Soc Interface 9(73):1757–1766. doi:10.1098/rsif.2012.0030

Nunes MC, Roy NS, Keyoung HM, Goodman RR, McKhann G, Jiang L, Kang J, Nedergaard M, Goldman SA (2003) Identification and isolation of multipotential neural progenitor cells from the subcortical white matter of the adult human brain. Nat Med 9(4):439–447. doi:10.1038/nm837

Pringle N, Collarini EJ, Mosley MJ, Heldin CH, Westermark B, Richardson WD (1989) PDGF A chain homodimers drive proliferation of bipotential (O-2A) glial progenitor cells in the developing rat optic nerve. EMBO J 8(4):1049

Rhee W, Ray S, Yokoo H, Hoane ME, Lee CC, Mikheev AM, Horner PJ, Rostomily RC (2009) Quantitative analysis of mitotic Olig2 cells in adult human brain and gliomas: implications for glioma histogenesis and biology. Glia 57(5):510–523. doi:10.1002/glia.20780

Roy NS, Wang S, Harrison-Restelli C, Benraiss A, Fraser RAR, Gravel M, Braun PE, Goldman SA (1999) Identification, isolation, and promoter-defined separation of mitotic oligodendrocyte progenitor cells from the adult human subcortical white matter. J Neurosci 19(22):9986–9995

Shih AH, Dai C, Hu X, Rosenblum MK, Koutcher JA, Holland EC (2004) Dose-dependent effects of platelet-derived growth factor-B on glial tumorigenesis. Cancer Res 64(14):4783–4789. doi:10.1158/0008-5472.can-03-3831

Swanson KR, Alvord EC, Murray JD (2000) A quantitative model for differential motility of gliomas in grey and white matter. Cell Prolif 33(5):317–329. doi:10.1046/j.1365-2184.2000.00177.x

Swanson KR, Alvord EC, Murray JD (2002) Virtual brain tumours (gliomas) enhance the reality of medical imaging and highlight inadequacies of current therapy. Br J Cancer 86(1):14–18. doi:10.1038/sj.bjc.6600021

Thorne RG, Hrabětová S, Nicholson C (2004) Diffusion of epidermal growth factor in rat brain extracellular space measured by integrative optical imaging. J Neurophysiol 92(6):3471–3481. doi:10.1152/jn.00352.2004

Westermark B, Heldin CH, Nister M (1995) Platelet-derived growth factor in human glioma. Glia 15(3):257–263. doi:10.1002/glia.440150307